Fang *et al. Chin. J. Mech. Eng.* (2021) 34:105
https://doi.org/10.1186/s10033-021-00624-w

Chinese Journal of Mechanical Engineering

ORIGINAL ARTICLE Open Access

Raising the Speed Limit of Axial Piston Pumps by Optimizing the Suction Duct

Yu Fang[1], Junhui Zhang[1*], Bing Xu[1], Zebing Mao[2], Changming Li[3], Changsheng Huang[1], Fei Lyu[1] and Zhimin Guo[4]

Abstract

The maximum delivery pressure and the maximum rotational speed determine the power density of axial piston pumps. However, increasing the speed beyond the limit always accompanies cavitation, leading to the decrease of the volumetric efficiency. The pressure loss in the suction duct is considered a significant reason for the cavitation. Therefore, this paper proposes a methodology to optimize the shape of the suction duct aiming at reducing the intensity of cavitation and increasing the speed limit. At first, a computational fluid dynamics (CFD) model based on the full cavitation model (FCM) is developed to simulate the fluid field of the axial piston pump and a test rig is set to validate the model. Then the topology optimization is conducted for obtaining the minimum pressure loss in the suction duct. Comparing the original suction duct with the optimized one in the simulation model, the pressure loss in the suction duct gets considerable reduction, which eases the cavitation intensity a lot. The simulation results prove that the speed limit can increase under several different inlet pressures.

Keywords: Axial piston pump, Speed limit, Topology optimization, Suction duct, Cavitation

1 Introduction

The axial piston pumps are widely used in hydraulic systems to provide the systems with pressurized fluid by converting the rotating mechanical power to hydraulic power [1]. An axial piston pump generally has odd numbers of pistons at equal angular intervals and each one is connected with a slipper by a ball joint. Figure 1 is the schematic diagram of its cross-section. When the main shaft rotating with the coupled cylinder block by spline, the displacement of the piston chambers starts to change, and the hydraulic oil is sucked or discharged through the valve plate, transmitting the hydraulic power.

The main advantages of the axial piston pumps are the high efficiency, available variable displacement, reliability, and most importantly, the high power density. However, in the past twenty years, the power density of axial piston pumps has not been significantly increased [2]. The pumps' power density is mainly limited by the maximum delivery pressure and the maximum rotational speed. Hence increasing the maximum speed is an effective method to improve it. But increasing the rotational speed will cause many problems, such as cavitation intensifying, flow ripple increase, tilting motion of rotating group, and heat problem [3]. In most cases of engineering practice, the cavitation phenomenon is the most likely to occur, which will decrease the volumetric efficiency and obstacle the further increase of the piston pumps' speed limit.

Cavitation is a dynamic process of gas cavity growth and collapse in a liquid. It can be categorized as gaseous cavitation and vaporous cavitation since the pressure is under the saturated pressure of the gas or the vapor pressure of liquid [4]. The former leads to air release from the fluid and bubbles arising while the latter results in low-pressure boiling and fluid vaporizing. In the oil-hydraulic piston pumps, the gaseous cavitation usually happens first therefore the saturated pressure of the gas is the

*Correspondence: benzjh@zju.edu.cn
[1] State Key Laboratory of Fluid Power and Mechatronic Systems, Zhejiang University, Hangzhou 310027, China
Full list of author information is available at the end of the article

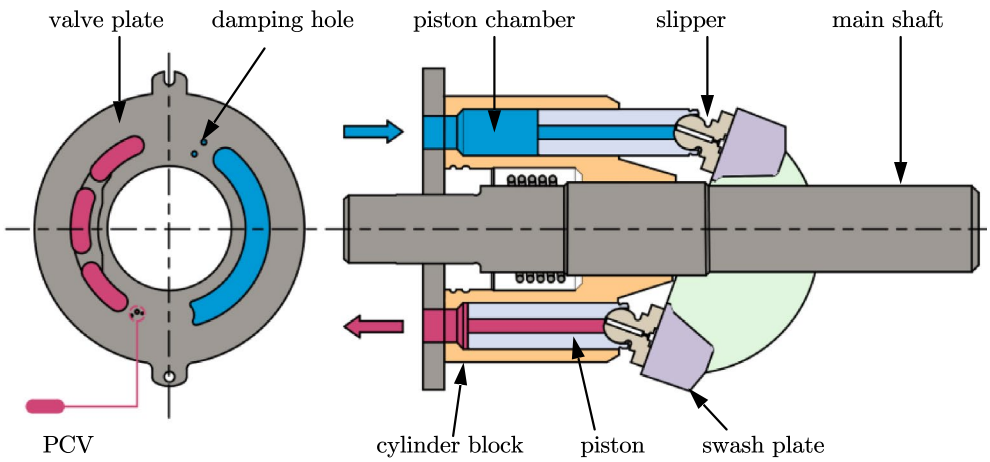

Figure 1 Schematic diagram of the axial piston pump

criterion to justify whether the cavitation occurs. When gaseous cavitation occurs, the air releases from the fluid, and the piston chambers become unfilled. Consequently, the delivery flow rate starts to decrease with the further increase of the rotational speed. The speed when the gaseous cavitation occurs is called the self-priming speed limit [2].

Many investigations have been made on the cavitation phenomenon for better design of the axial piston pumps. Harris [5] used different air-release and cavitation models to discuss the suction performance of high-speed axial piston pumps. But this model was just a simplified single-cylinder system. Bernhard [6] built a mathematical model of the complex suction system which comprises wave propagation in pipes and hoses, a detailed model of the pump including each of its nine cylinders, cavitation therein, the charge and discharge processes of these cylinders with the suction duct, and several accessories influencing the hydraulic process. With the evolution and innovation of computational fluid dynamics (CFD) technologies in the last decades, the novel CFD methodology and multiple cavitation models of the axial piston pumps were presented and validated [7–9], which further improved the accuracy for both cavitation and performance predictions.

There are two main reasons for pressure drop bringing about the cavitation phenomenon. The first one is the flow inverse in the transition region of the valve plate where the piston chambers start to compress or decompress, which will form jet flow in the relief groove of the valve plate leading to the cavitation near the relief groove and the cylinder ports [10]. Besides, the inverse flow will also arouse the pressure undershoot of the piston chambers, which almost increases proportionally to the rotational speed [5]. Some research has been conducted on optimizing the geometry of the valve plate to suppress the inverse flow and thus ease the cavitation intensity [11, 12]. The auxiliary pre-expansion volume (PEV) [13] and the pre-compression volume (PCV) [14] connected to the valve plate were also introduced to reduce the inverse flow.

Another reason for pressure drop is the pressure loss in the suction duct due to the flow resistance. An effective way is to increase the inlet pressure [15, 16], such as adding a boosting device, but it is generally expensive and decreases the power density. Therefore, some researchers have improved the suction performance by changing the angle of the inlet port of the suction duct [17] and proposing a kind of bionic design of the suction duct based on meandering rivers [18]. However, the previous optimizations on the suction duct are just empirical methods. In this paper, topology optimization is used to reduce the pressure loss in the suction duct to the minimum, aiming at preventing cavitation.

This study includes the following contents. Firstly, a CFD model of the piston pump based on the full cavitation model (FCM) is established and a test rig is set up to validate the model. Then a topology methodology is developed to optimize the suction duct for reducing the pressure loss. Finally, the optimized result is compared to the original one. The pressure loss in the suction duct and the cavitation intensity both show a considerable reduction, and the speed limit improves a lot.

2 CFD Modeling

The axial piston pump studied in this paper is HPR-02-210 manufactured by Linde Hydraulics (China) Co., Ltd. A CFD model of this piston pump based on the FCM will be established in this section by CFD software.

2.1 Full Cavitation Model

The cavitation model can be categorized as the homogeneous mixture model and the three-component two phase flow model [19]. The former model ignores the influence of the non-condensable gas on cavitation as well as the velocity slip between the vapor and the liquid, while the latter takes such factors into account [20]. For engineering application in axial piston pumps, the velocity in the low-pressure region is relatively high and the velocity slip between the vapor and the liquid is rather small. Besides, what we care about most in this study is the total gas fraction. The process of the phase transition influenced by the non-condensable gas is negligible. As a result, the FCM as a homogeneous mixture model is selected to simulate the cavitation phenomenon in this study.

According to the study of Singhal et. al [20], the FCM accounts for all three first-order effects of the formation of transport of vapor bubbles, the turbulent fluctuations of pressure and velocity, and the magnitude of non-condensable gases. The vapor mass fraction f is governed by a transport equation:

$$\frac{\partial}{\partial t}(\rho f) + \nabla \cdot (\rho \boldsymbol{v} f) = \nabla \cdot (\Gamma \nabla f) + R_e - R_c, \tag{1}$$

where $\boldsymbol{v}$ is the fluid velocity vector, ρ is the density of the fluid mixture, R_e and R_c are the vapor generation and condensation rates respectively. In the CFD model, the equation can be rewritten in integral form as:

$$\begin{aligned} &\frac{\partial}{\partial t}\int_{\Omega(t)} \rho f \mathrm{d}\Omega + \int_{\sigma} \rho((\boldsymbol{v} - \boldsymbol{v}_\sigma)\cdot \boldsymbol{n}) f \mathrm{d}\sigma = \\ &\int_{\sigma} \left(D_f + \frac{\mu_t}{\sigma_f}\right)(\nabla f \cdot \boldsymbol{n})\mathrm{d}\sigma + \int_{\Omega} (R_e - R_c)\mathrm{d}\Omega, \end{aligned} \tag{2}$$

where Ω is the control volume, σ is the surface of control volume, $\boldsymbol{n}$ is the surface norm D_f is the diffusivity of vapor mass fraction, μ_t is the turbulent viscosity, σ_f is the turbulent Schmidt number.

The vapor generation term R_e and the condensation rate term R_c are modeled as:

$$R_e = C_e \frac{\sqrt{k}}{\sigma_l}\rho_l \rho_v \left[\frac{2}{3}\frac{(p - p_v)}{\rho_l}\right]^{1/2}(1 - f_v - f_g), \tag{3}$$

$$R_c = C_c \frac{\sqrt{k}}{\sigma_l}\rho_l \rho_v \left[\frac{2}{3}\frac{(p - p_v)}{\rho_l}\right]^{1/2} f_v, \tag{4}$$

where k is the turbulence kinetic energy, σ_l is the surface tension, ρ_l and ρ_v are the density of the liquid and gas, p is the liquid pressure, p_v is the vaporous pressure, f_v is the vapor mass fraction, f_g is the non-condensable gas fraction. The empirical coefficient C_e and C_c are 0.02 and 0.01 respectively which are satisfactory for general use according to the study by Singhal [20] and Ding [11]. In this CFD model, the turbulence model is the standard $k - \varepsilon$ model.

The non-condensable gas density ρ_g is calculated by the perfect gas law:

$$\rho_g = \frac{WP}{RT}. \tag{5}$$

Finally, the density of the fluid mixture is calculated by:

$$\frac{1}{\rho} = \frac{f_v}{\rho_v} + \frac{f_g}{\rho_g} + \frac{1 - f_v - f_g}{\rho_l}. \tag{6}$$

2.2 CFD Model Grid Division and Parameter Set

To establish the CFD model, the flow field of the piston pump should be extracted from the CAD model first then imported into the CFD software. The motion of the pistons includes the rotation around the main shaft and the translation along the piston chambers, while the remaining volumes keep still. An inner mesh template of axial piston pumps in the software creates structural hex mesh for the pistons. The remaining still volumes are divided into general mesh promising enough accuracy. Besides, the interface between the adjacent volumes where the fluid flows through is also created by another mesh template. The result of the grid division is shown in Figure 2. The parameters set in the CFD model are shown in Table 1.

In this paper, all the computational results are obtained after 5 revolutions and stable with the simulation time.

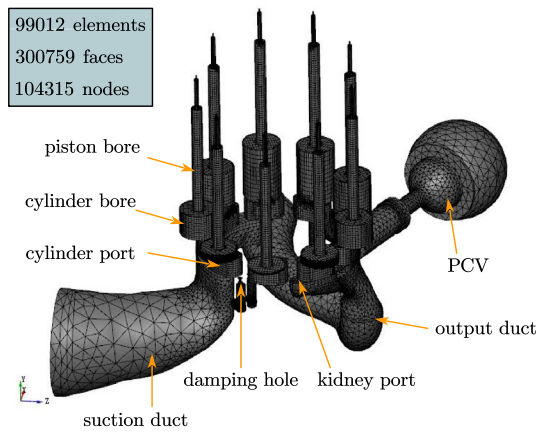

Figure 2 Mesh result of the fluid field of the axial piston pump

Table 1 Parameter setting in the CFD model

Parameter	Value
Displacement (mL/r)	210
Number of pistons	9
Piston radius (mm)	27
Swash-plate angle (°)	20
Delivery pressure (MPa)	20
Fluid temperature (℃)	40
Fluid density (kg/m^3)	856
Dynamic viscosity (Pa·s)	0.0296
Fluid bulk modulus (GPa)	1.51
Gas mass fraction	9×10^{-5}
Air-release pressure (MPa)	0.101
Vaporous pressure (MPa)	7.4×10^{-3}
Gas density (kg/m^3)	1.29
Vapor density (kg/m^3)	0.0245

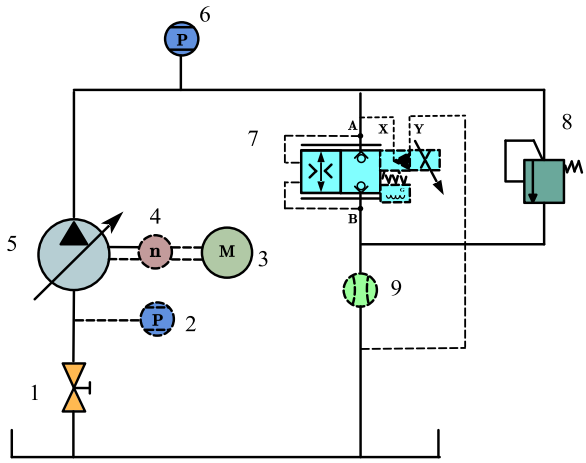

Figure 3 Schematics of the hydraulic circuit

3 Experiment

3.1 Test Rig

To validate the CFD model, a test rig is set up. The experimental schematic of the hydraulic circuit and the picture of the test rig are shown in Figures 3 and 4, respectively. The inlet pressure is regulated by a globe valve 1 while the delivery pressure is controlled by a proportional throttle valve 7 which has pressure feedback. The relief valve 8 is used to limit the delivery pressure for safety. Furthermore, the shaft speed sensor 4, pressure sensors 2 and 6, and flowmeter 9 are equipped in the hydraulic system to measure the relevant parameters. A mounting hole has been drilled on the test pump and pressure sensor 2 is mounted in the hole to test the inlet pressure. In the experiment, the delivery pressure is set as 20 MPa,

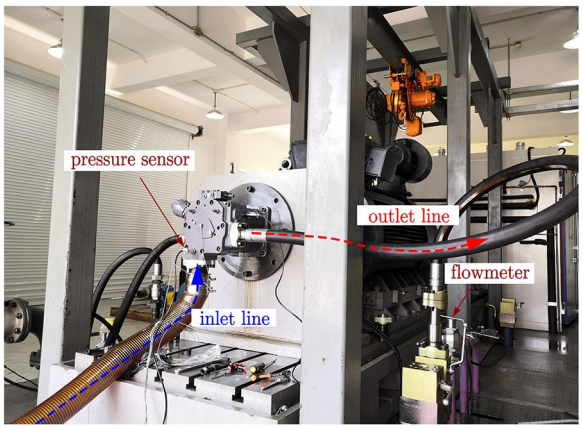

Figure 4 Picture of the test rig

Table 2 Details of the hydraulic system

No.	Description	Detail
1	Globe valve	Manual adjustment
2	Pressure sensor	0–6 MPa, accuracy ± 0.5%
3	Electrical motor	0–5000 r/min
4	Shaft speed sensor	0–3000 r/min, accuracy ± 0.5%
5	Test pump	210 mL/r
6	Pressure sensor	0–60 MPa, accuracy ± 0.5%
7	Proportional throttle valve	0–35 MPa
8	Relief valve	0–35 MPa
9	Flowmeter	0–600 L/min, accuracy ± 0.5%

similar to the CFD model. The details of the hydraulic system are listed in Table 2.

3.2 Experimental Results and Discussion

Regulate the globe valve to set the inlet pressure as 0.05 MPa, 0.07 MPa, and 0.1 MPa, the speed limit varies. It is needed to point out that the inlet pressures in both simulation and experiment are gauge pressure. Figure 5 shows the relationship between rotational speed and the delivery flow rate under different inlet pressures. As the rotational speed increases, the flow rate improves proportionally at the beginning and the ratio of the flow rate to the rotational speed is just the displacement of the pump. However, once the speed exceeds the limit, the delivery flow rate starts to increase slowly than before and then decreases, indicating the descend of the volumetric efficiency. The experimental results demonstrate that the inlet pressure has a great influence on the speed limit, the lower the inlet pressure, the lower the speed limit. Therefore, it is useful to reduce the pressure loss by optimizing the suction duct to increase the speed limit.

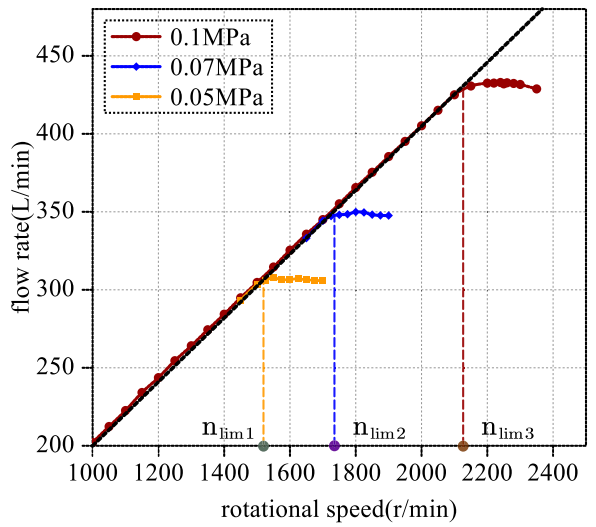

Figure 5 Relationship of the rotational speed and the delivery flow rate under different inlet pressures

3.3 Validation of the CFD model

The delivery flow rate under different rotational speeds in the CFD model and test rig is shown in Figure 6, and three different inlet pressures are considered. The simulation results of the delivery flow rate show consistency with the experiment before the speed limit. The error comes from the leakage and the error of the FCM. When the rotational speed is under the speed limit, the cavitation phenomenon has not happened, and the error comes from mainly the leakage flow rate, which is not considered in the CFD model. So the simulated flow rate is higher than the experimental value. When the rotational speed is beyond the speed limit, the error is influenced by both the leakage and the FCM. The flow rate predicted by the cavitation model is generally lower than the experimental value, and as the rotational speed increases, the simulated flow rate becomes lower and lower. Therefore, as the rotational speed just starts to increase beyond the limit, the total error does not increase but decreases instead.

However, the error in the CFD model is acceptable since the maximum is less than 3%, and the speed limits in simulation and experiment are coincident. Therefore, we can use this model to predict the speed limit and observe the cavitation phenomenon.

4 Topology Optimization

The fundamental goal of the topology optimization method is to obtain the best structural performance by properly placing material within a prescribed design domain [21]. This method originates from the field of solid mechanics by the end of the 1980s and then spreads to a range of different disciplines such as acoustics [22], photonics [23], electromagnetism [24], heat condition [25], and fluid flow [26], etc. Nowadays topology optimization is available in all major finite element analysis packages and even in many computer-aided design packages. Some researchers have made use of this method to reduce the structural vibration and noise of the axial piston pumps [27]. In this paper, the topology optimization is conducted on the suction duct to obtain the minimum pressure loss.

4.1 Mathematical Model

Before we start the process of optimization, the mathematical model of topology optimization is needed to be established. Generally, the topology optimization problem is [28]:

$$\begin{aligned} &\min_{\gamma} J(\boldsymbol{U}(\gamma),\gamma) \\ &\text{s.t.}, \boldsymbol{R}(\boldsymbol{U}(\gamma),\gamma)=0, \\ &g_i(\gamma)\le 0,\ \forall i=1,...,N, \\ &0\le\gamma\le 1, \end{aligned} \tag{7}$$

where $J(\cdot)$ is the objective function, γ is the optimization design variable, $\boldsymbol{R}$ is the vector of governing equations

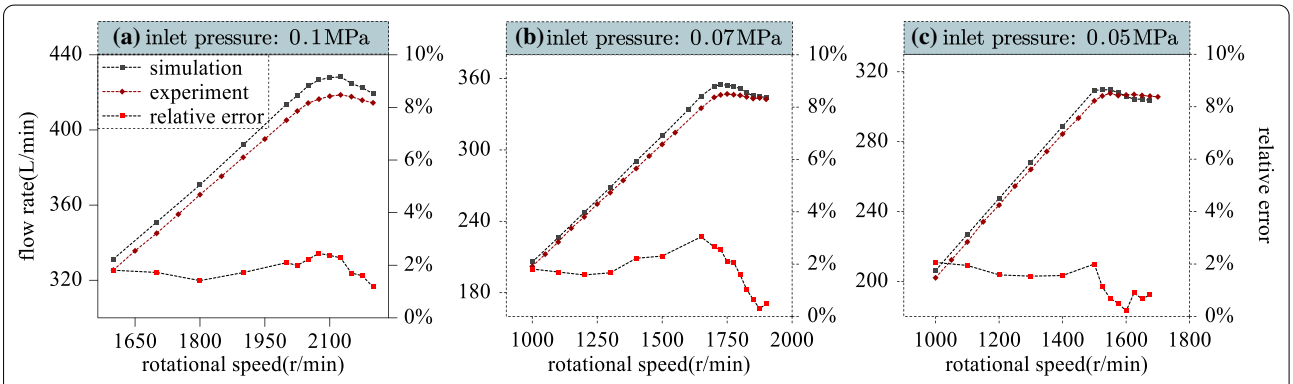

Figure 6 Simulation and experimental results of the delivery flow rate under different rotational speeds

written in residual form, and g_i is a set of inequality constraints.

In this study, the goal is to optimize the suction duct to obtain the minimum pressure loss. So the dissipated energy in the design domain is chosen to be the objective function [29], which can be calculated as [30]:

$$J(\boldsymbol{u};\gamma) = \int_0^T \int_\Omega \left[\frac{\eta}{2}\left(\nabla\boldsymbol{u}+\nabla\boldsymbol{u}^{\mathrm{T}}\right):\left(\nabla\boldsymbol{u}+\nabla\boldsymbol{u}^{\mathrm{T}}\right)+\alpha\boldsymbol{u}^2\right]\mathrm{d}\Omega\mathrm{d}T, \tag{8}$$

where $\boldsymbol{u}$ is the fluid velocity and η is the fluid viscosity. Ω is the initial design domain as shown in Figure 7(b). α is the impermeability of a porous medium whose value depends on the optimization design variable γ by an interpolation function:

$$\alpha(\gamma) = \alpha_{\min} + (\alpha_{\max} - \alpha_{\min})\frac{q(1-\gamma)}{q+\gamma}, \tag{9}$$

and q is a real and positive parameter used to adjust the convexity of the interpolation function. γ is the optimization design variable, and it is the artificial density of the design domain. During the iteration process, γ varies between 0 and 1, where 0 represents the solid domain and 1 is the fluid domain.

The flow in the suction duct is governed by the Navier-Stokes (NS) equation. We neglect the compressibility of the fluid in this study, and the N-S equation can be written as:

$$\begin{aligned}&\rho\frac{\partial\boldsymbol{u}}{\partial t} - \eta\nabla\cdot\left(\nabla\boldsymbol{u}+\nabla\boldsymbol{u}^{\mathrm{T}}\right)+\rho(\boldsymbol{u}\cdot\nabla)\boldsymbol{u}+\nabla p = \boldsymbol{f}, \text{in } \Omega,\\ &-\nabla\cdot\boldsymbol{u} = 0, \text{in } \Omega,\end{aligned} \tag{10}$$

where $\boldsymbol{f}$ is the body force and can be expressed as:

$$\boldsymbol{f} = -\alpha\boldsymbol{u}. \tag{11}$$

To solve the N-S equation, several boundary conditions need to be added. The inlet pressure is set as 0.1 MPa, and the flow direction is perpendicular to the inlet and outlet port.

$$p = 0.1 \text{ MPa}, \text{ on } \Gamma_{NI}, \tag{12}$$

$$\boldsymbol{u}\times\boldsymbol{n} = 0, \text{ on } \Gamma_{NI} \text{ and } \Gamma_{NO}, \tag{13}$$

where Γ_{NI} and Γ_{NO} are the inlet and outlet port, respectively.

The no-slip boundary condition is also considered as:

$$\boldsymbol{u} = 0, \text{ on } \Gamma_D, \tag{14}$$

where Γ_D is the boundary of the suction duct.

The outlet of the suction duct is an open-boundary. So, the stress distributed on the boundary Γ_{NO} is:

$$\left[-p\boldsymbol{I}+\eta\left(\nabla\boldsymbol{u}+\nabla\boldsymbol{u}^{\mathrm{T}}\right)\right]\boldsymbol{n} = 0, \text{ on } \Gamma_{NO}. \tag{15}$$

There are also several constraints of this optimization, including the volume constraint and the shape constraints of the inlet and outlet port.

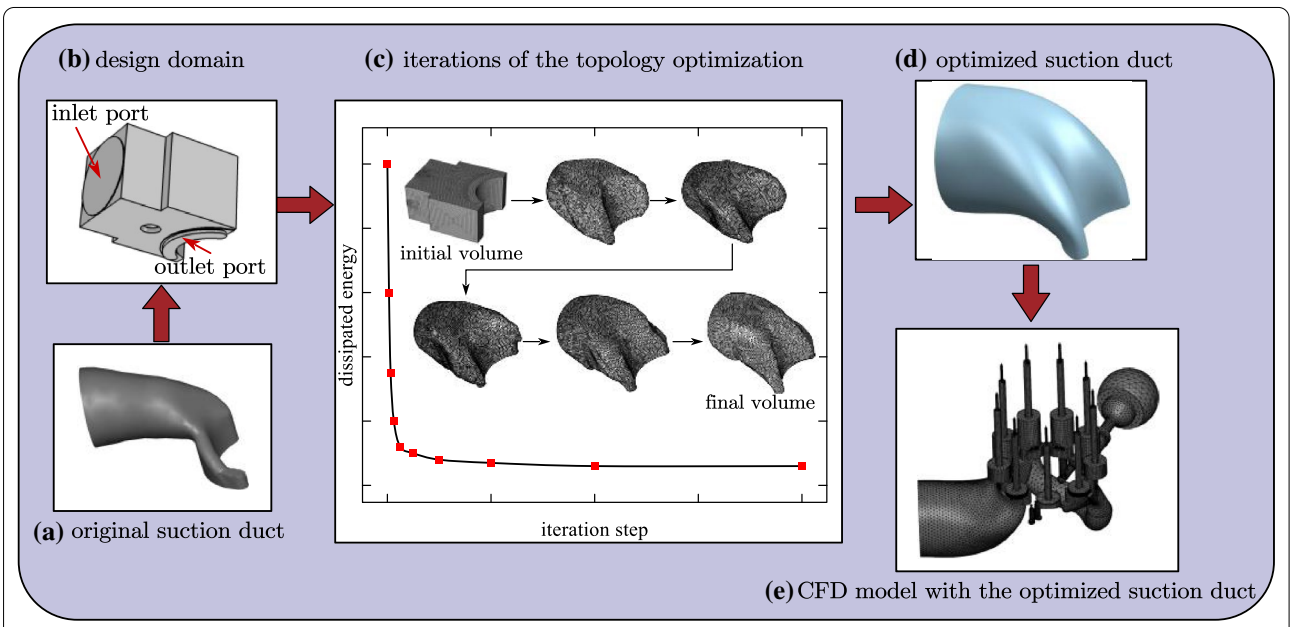

Figure 7 Process of the topology optimization

$$\int_{\Omega} \gamma \mathrm{d}\Omega \leq \theta V, \tag{16}$$

$$\gamma = 1, \quad \text{on } \Gamma_{NI} \text{ and } \Gamma_{NO}, \tag{17}$$

where V is the total volume of the design domain and θ is the prescribed fluid volume fraction.

According to the objective function, boundary conditions, and constraints discussed above, the mathematical model of this topology optimization problem can be written as:

$$\begin{aligned}
&\min : J(\boldsymbol{u}, p; \gamma) = \\
&\int_0^T \int_{\Omega} \left[\frac{\eta}{2} \left(\nabla \boldsymbol{u} + \nabla \boldsymbol{u}^{\mathrm{T}} \right) : \left(\nabla \boldsymbol{u} + \nabla \boldsymbol{u}^{\mathrm{T}} \right) + \alpha \boldsymbol{u}^2 \right] \mathrm{d}\Omega \mathrm{d}T, \\
&\text{s.t.,} \ \rho \frac{\partial \boldsymbol{u}}{\partial t} - \eta \nabla \cdot \left(\nabla \boldsymbol{u} + \nabla \boldsymbol{u}^{\mathrm{T}} \right) + \rho (\boldsymbol{u} \cdot \nabla) \boldsymbol{u} + \nabla p = -\alpha \boldsymbol{u}, \text{in } \Omega, \\
&-\nabla \cdot \boldsymbol{u} = 0, \text{in } \Omega, \\
&p = 0.1 \text{ MPa}, \text{on } \Gamma_{NI}, \\
&\boldsymbol{u} \times \boldsymbol{n} = 0, \text{on } \Gamma_{NI} \text{ and } \Gamma_{NO}, \\
&\left[-p\boldsymbol{I} + \eta \left(\nabla \boldsymbol{u} + \nabla \boldsymbol{u}^{\mathrm{T}} \right) \right] \boldsymbol{n} = 0, \text{on } \Gamma_{NO}, \\
&\boldsymbol{u} = 0, \text{on } \Gamma_{D}, \\
&\int_{\Omega} \gamma \mathrm{d}\Omega \theta V \gamma = 1, \quad \text{on } \Gamma_{NI} \text{ and } \Gamma_{NO}, \\
&\alpha(\gamma) = \alpha_{\min} + \left(\alpha_{\max} - \alpha_{\min} \right) \frac{q(1-\gamma)}{q+\gamma}.
\end{aligned} \tag{18}$$

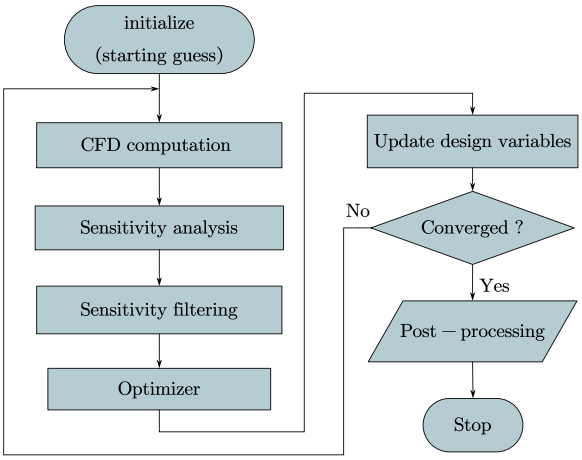

Figure 8 Flow-chart of computations for topology optimization

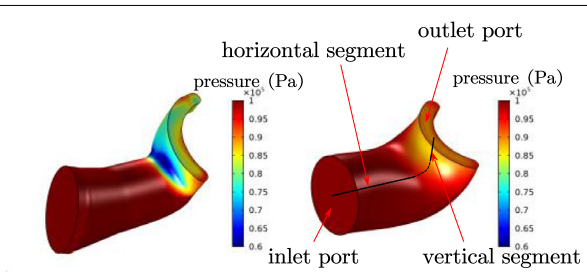

Figure 9 Pressure distribution of the original and optimized suction duct

4.2 Process of the Topology Optimization

The process of the whole topology optimization is shown in Figure 7, and the flow-chart of computation for topology optimization is shown in Figure 8. The steps to run the optimization require first to define an initial material distribution. Then the CFD computation is conducted to get the flow characteristics and calculate the dissipated energy under the initial guess. Next, we calculate the sensitivities by the adjoint method. The sensitivity information is used to compute the next design material distribution, i.e., update the design variables by the optimizer. But before that, the step of sensitivity filtering is needed to suppress the problems like chessboard, mesh dependency, and grey transition [31]. The optimizer chosen in this optimization is the widely used method of moving asymptotes (MMA). If the updated design variables are not converged, the above process needs to be conducted again. The material distribution of the process of the iterations is shown in Figure 7(c).

After the design variables converge, the final volume is still coarse and needs post-processing. To smoothen the boundary, the NURBS spline is used to fit it in 3D CAD software. The optimized suction duct after fitting is shown in Figure(d).

At last, the original suction duct is replaced by the optimized one in the CFD model to simulate again.

4.3 Optimization Results and Discussion

Figure 9 shows the contrast of the pressure distribution between the original and optimized suction duct, which demonstrates that the optimized suction duct has less pressure loss. During the suction phase of the piston pump, the two main factors accounting for the pressure loss are the frictional pressure loss and the local pressure loss.

As shown in Figure 9, both original and optimized suction duct can be divided into three parts, the horizontal segment, the vertical segment, and the transition area. In the original suction duct, the flow velocity in the horizontal segment is much faster than the optimized one as shown in Figures 10 and 11, leading to a bigger viscous resistance and therefore more frictional pressure loss.

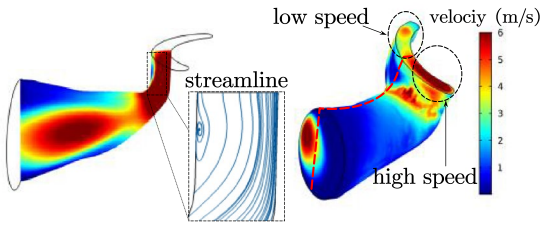

Figure 10 Velocity distribution of the original suction duct

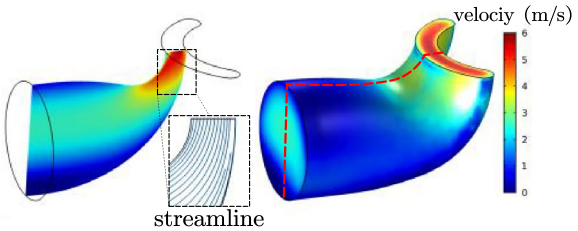

Figure 11 Velocity distribution of the optimized suction duct

Besides, in the transition area, the original suction duct has a sharper turn than the optimized one. A portion of the fluid cannot follow the main flow in this region, so the flow separation occurs. As shown in Figure 10, the portion of slow fluid forms a vortex in this region and consistently dissipates energy, causing a local pressure loss.

The pressure loss in the suction duct gives rise to the cavitation phenomenon and the generated bubbles will be sucked into the piston chambers in the suction phase. Therefore, the piston pump cannot deliver enough fluid in the discharge phase, leading to a decrease of the volumetric efficiency and the speed limit.

Additionally, as shown in Figures 10 and 11, the velocity on the outlet port of the original suction duct is not well-distributed compared to the optimized one. In the low speed region shown in Figure 10, the piston chambers of the piston pump are not able to suck enough fluid. As a result, the pressure in the piston chambers drops off, which may also cause cavitation.

Comparing to the original one, the diameter of the optimized suction duct in the horizontal segment changes slowly, and the curvature in the transition area is smoother. Therefore, the fractional and local pressure loss are both reduced a lot. Furthermore, the velocity on the outlet of the optimized suction duct is well-distributed. On the whole, the topology optimization on the suction duct can reduce the cavitation intensity and improve the speed limit.

Corresponding to the experimental data, three different inlet pressures, 0.1 MPa, 0.07 MPa, and 0.05 MPa, are set in the CFD model to simulate the cavitation intensity and the speed limit. Figure 12 shows the comparisons of the gas volume fraction in the piston chamber with the original and optimized suction duct. The cavitation region with the optimized suction duct is smaller than the original one under all three inlet pressures. The results indicate that the optimized suction duct can effectively reduce the cavitation intensity under different inlet pressures. Consequently, the optimized suction duct increases the delivery flow rate at a relatively high rotational speed as shown in Figure 13. And the speed limit of the axial piston pump is improved with it. The simulation results prove the effectiveness of the topology optimization method on increasing the speed limit of the axial piston pumps.

5 Conclusions and Outlook

In this paper, the topology optimization method was conducted on the suction duct of the axial piston pump to increase the speed limit. The CFD model was established firstly, then a test rig was built up to validate it. Finally, the simulation result proved the effectiveness of the topology optimization. Based on the experiment and simulation in this paper, the following conclusions can be drawn.

(1) From the experimental results, the volumetric efficiency will decrease if the rotational speed exceeds the speed limit. The speed limit is influenced by the inlet pressure of the axial piston pump. As the inlet pressure decreases, the speed limit decreases.
(2) The main factors of the pressure loss in the suction duct are frictional and local pressure loss, including the flow separation and turbulent vortex.
(3) The simulation results proved that the topology optimization on the suction duct can effectively improve the speed limit. The pressure loss in the optimized suction duct was reduced a lot, which eased the intensity of the cavitation phenomenon. Finally, the speed limit improved with it.

Owing to the high cost of manufacturing the piston pump with an optimized suction duct, the experiment on the optimized suction duct has not been conducted. However, this paper has shown the enormous potential of topology optimization on piston pumps. In future work, this method can be applied more widely to designing the flow duct of various hydraulic pumps and motors.

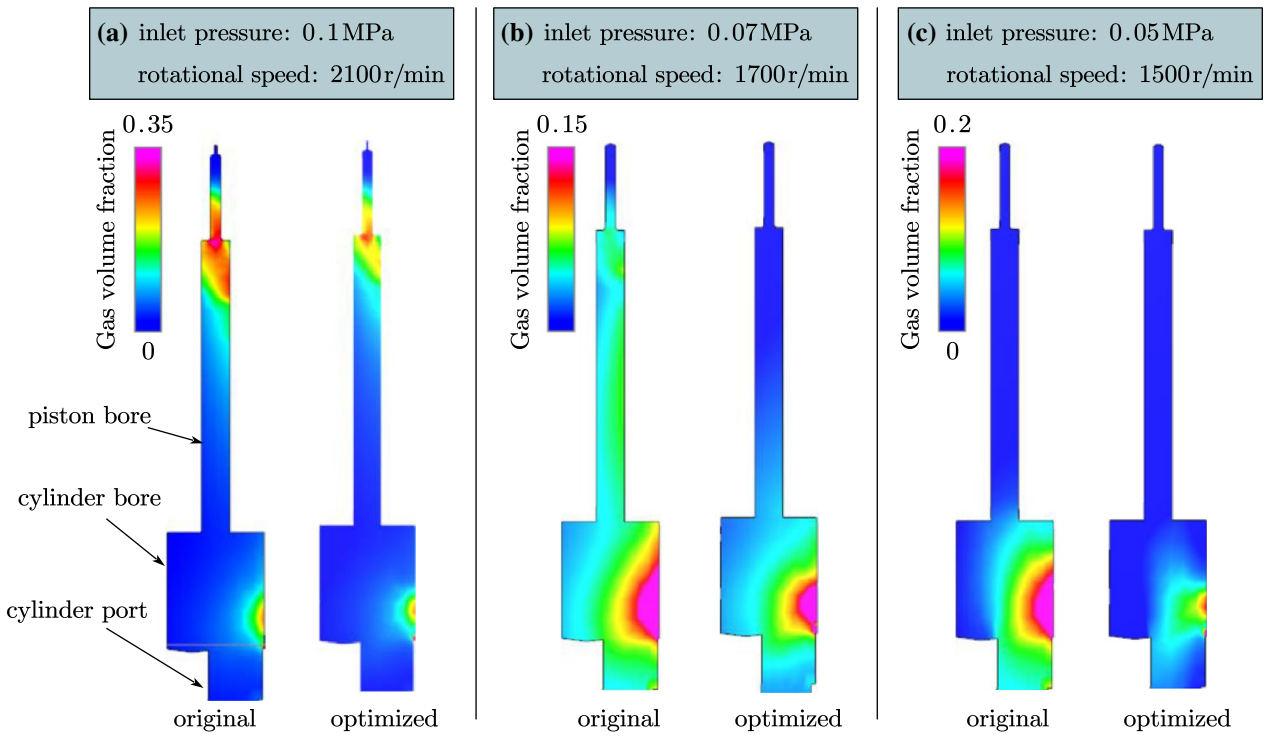

Figure 12 Comparison of the two-dimensional cavitation region in the piston chamber with the original and optimized suction duct

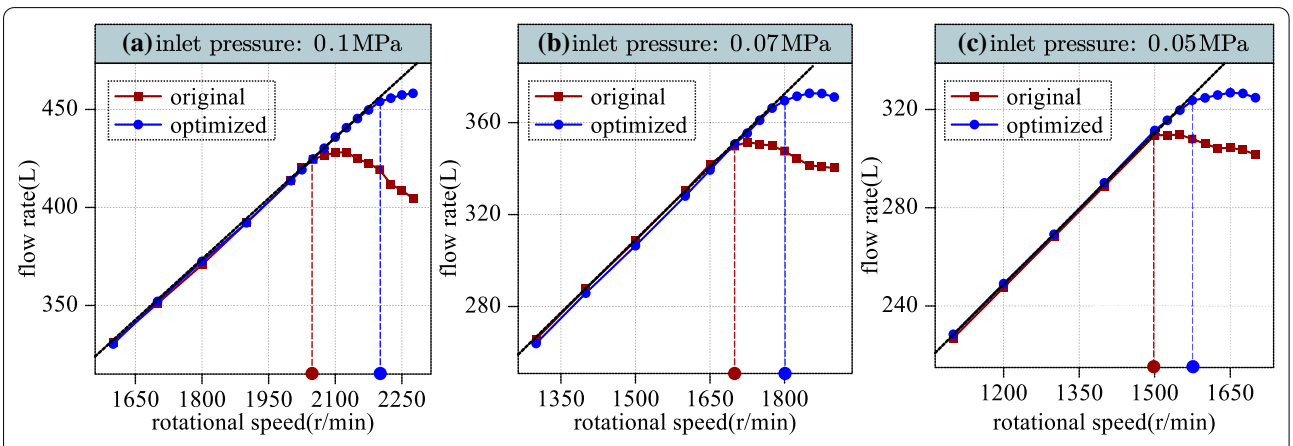

Figure 13 Comparison of the delivery flow rate with the original and optimized suction duct

Acknowledgments
The authors sincerely thank the National Intelligent Manufacturing Equipment Quality Supervision and Inspection Center (Zhejiang) for providing the test rig in this study.

Authors' contributions
BX and JZ were in charge of the whole trial; YF and ZM wrote the manuscript; CL, CH, FL, and ZG assisted with experiment and data analyses. All authors read and approved the final manuscript.

Authors' Information
Yu Fang, born in 1999, is currently a master candidate at *State Key Laboratory of Fluid Power and Mechatronic Systems, Zhejiang University, China*. He received his bachelor's degree from *Central South University, China*, in 2020. His research interests include the cavitation and vibro-acoustics of axial piston pumps.
Junhui Zhang, born in 1983, is currently a professor at *State Key Laboratory of Fluid Power and Mechatronic Systems, Zhejiang University, China*. His main research interests are fluid power transmission and control, and noise control of axial piston machines.

Bing Xu, born in 1971, is currently a professor and a Ph.D. candidate supervisor at *State Key Laboratory of Fluid Power and Mechatronic Systems, Zhejiang University, China*. His main research interests are fluid power transmission and control, and noise control of axial piston machines.
Zebing Mao, is currently an assistant professor at *Department of Engineering Science and Mechanics, Shibaura Institute of Technology, Japan*.
Changming Li, born in 1974, is currently an engineer at *Hangzhou Optimax Tech Co., Ltd., China*.
Changsheng Huang, born in 1996, is currently a master candidate at *State Key Laboratory of Fluid Power and Mechatronic Systems, Zhejiang University, China*.
Fei Lyu, born in 1996, is currently a Ph.D. candidate at *State Key Laboratory of Fluid Power and Mechatronic Systems, Zhejiang University, China*.
Zhimin Guo, is currently an engineer at *Hydraulic Transmission Institute, Linde Hydraulic, China*. His main research interests are hydraulic pumps, motors and valves development.

Funding
Supported by National Key R&D Program of China (Grant No. 2019YFB2004504).

Competing interests
The authors declare no competing financial interests.

Author Details
[1]State Key Laboratory of Fluid Power and Mechatronic Systems, Zhejiang University, Hangzhou 310027, China. [2]Department of Engineering Science and Mechanics, Shibaura Institute of Technology, Tokyo, Japan. [3]Hangzhou Optimax Tech Co.,Ltd, Hangzhou, China. [4]Linde Hydraulics (China) Co., Ltd, Weifang 261000, China.

Received: 5 April 2021 Revised: 16 July 2021 Accepted: 13 October 2021
Published online: 12 November 2021

References

[1] Jiang'ao Z, Yongling Fu, Jiming Ma, et al. Review of cylinder block/valve plate interface in axial piston pumps: Theoretical models, experimental investigations, and optimal design. *Chinese Journal of Aeronautics*, 2021, 34(1): 111-134.
[2] M Kunkis, J Weber. Experimental and numerical assessment of an axial piston pump's speed limit. *Proceedings of the BATH/ASME 2016 Symposium on Fluid Power and Motion Control. BATH/ASME 2016 Symposium on Fluid Power and Motion Control*, Bath, UK, September 7–9, 2016.
[3] Q Chao, J Zhang, B Xu, et al. A review of high-speed electro-hydrostatic actuator pumps in aerospace applications: challenges and solutions. *Journal of Mechanical Design*, 2019, 141(5): 050801.
[4] S Gullapalli, P Michael, J Kensler, et al. An investigation of hydraulic fluid composition and aeration in an axial piston pump. *Fluid Power Systems Technology, American Society of Mechanical Engineers*, 2017, 58332: V001T01A028.
[5] R M Harris, K A Edge, D G Tilley. The suction dynamics of positive displacement axial piston pumps. *Journal of Dynamic Systems, Measurement and Control: Transactions of the ASME*, 1994, 116(2): 281-287.
[6] B Manhartsgruber, R Scheidl. Cavitation driven impact in a hydraulic piston pump: A theoretical and experimental investigation. *International Design Engineering Technical Conferences and Computers and Information in Engineering Conference*, American Society of Mechanical Engineers, 1997: 80432.
[7] A Iannetti, M T Stickland, W M Dempster. A CFD and experimental study on cavitation in positive displacement pumps: Benefits and drawbacks of the 'full' cavitation model. *Engineering Applications of Computational Fluid Mechanics*, 2016, 10(1): 57-71.
[8] B Zhao, W Guo, L Quan. Cavitation of a submerged jet at the spherical valve plate/cylinder block interface for axial piston pump. *Chinese Journal of Mechanical Engineering*, 2020, 33(1): 1-15.
[9] H Ding, F C Visser, Y Jiang, et al. Demonstration and validation of a 3D CFD simulation tool predicting pump performance and cavitation for industrial applications. *Journal of Fluids Engineering*, 2011, 133(1): 011101.
[10] T Tsukiji, N K akayama, K Saito, et al. Study on the cavitating flow in an oil hydraulic pump. *Proceedings of 2011 International Conference on Fluid Power and Mechatronics*, IEEE, 2011: 253-258.
[11] S Ye, J Zhang, B Xu. Noise reduction of an axial piston pump by valve plate optimization. *Chinese Journal of Mechanical Engineering*, 2018, 31: 57.
[12] W Sang. The analysis of cavitation problems in the axial piston pump. *Journal of Fluids Engineering*, 2010, 132(7): 074502.
[13] B Xu, S Ye, J Zhang, et al. Flow ripple reduction of an axial piston pump by a combination of cross-angle and pressure relief grooves: Analysis and optimization. *Journal of Mechanical Science and Technology*, 2016, 30(6): 2531-2545.
[14] B Xu, Y Song, H Yang. Pre-compression volume on flow ripple reduction of a piston pump. *Chinese Journal of Mechanical Engineering*, 2013, 26(6): 1259-1266.
[15] N D Manring, V S Mehta, B E Nelson, et al. Scaling the speed limitations for axial-piston swash-plate type hydrostatic machines. *Journal of Dynamic Systems, Measurement and Control: Transactions of the ASME*, 2014, 136(3): 031004.
[16] F Yin, S Nie, X Siao, et al. Numerical and experimental study of cavitation performance in sea water hydraulic axial piston pump. *Proceedings of the Institution of Mechanical Engineers, Part I: Journal of Systems and Control Engineering*, 2016, 230(8): 716–735.
[17] N Bügener, S Helduser. Analysis of the suction performance of axial piston pumps by means of computational fluid dynamics (CFD). *Seventh International Fluid Power Conference*, Aachen, Germany, 2010: 22-24.
[18] N Bügener, J Klecker, J Weber. Analysis and improvement of the suction performance of axial piston pumps in swash plate design. *International Journal of Fluid Power*, 2014, 15(3): 153-167.
[19] X Luo, B Ji, Y Tsujimoto. A review of cavitation in hydraulic machinery. *Journal of Hydrodynamics*, 2016, 28(3): 335-358.
[20] A K Singhal, M M Athavale, H Li, et al. Mathematical basis and validation of the full cavitation model. *Journal of Fluids Engineering*, 2002, 124(3): 617-624.
[21] O Sigmund, K Maute. Topology optimization approaches. *Structural and Multidisciplinary Optimization*, 2013, 48(6): 1031-1055.
[22] C B Dilgen, S B Dilgen, N Aage, et al. Topology optimization of acoustic mechanical interaction problems: A comparative review. *Structural and Multidisciplinary Optimization*, 2019, 60(2): 779-801.
[23] W Li, F Meng, Y Chen, et al. Topology optimization of photonic and phononic crystals and metamaterials: A review. *Advanced Theory and Simulations*, 2019, 2(7): 1900017.
[24] S Zhou, W Li, Q Li. Level-set based topology optimization for electromagnetic dipole antenna design. *Journal of Computational Physics*, 2010, 229(19): 6915-6930.
[25] T Dbouk. A review about the engineering design of optimal heat transfer systems using topology optimization. *Applied Thermal Engineering*, 2017, 112: 841-854.
[26] J Alexandersen, C S Andreasen. A review of topology optimisation for fluid-based problems. *Fluids*, 2020, 5(1): 29.
[27] B Xu, S Ye, J Zhang. Numerical and experimental studies on housing optimization for noise reduction of an axial piston pump. *Applied Acoustics*, 2016, 110: 43-52.
[28] C B Dilgen, S B Dilgen, D R Fuhrman, et al. Topology optimization of turbulent flows. *Computer Methods in Applied Mechanics and Engineering*, 2018, 331: 363-393.
[29] T Borrvall, J Petersson. Topology optimization of fluids in Stokes flow. *International Journal for Numerical Methods in Fluids*, 2003, 41(1): 77-107.
[30] Y Deng, Z Liu, P Zhang, et al. Topology optimization of unsteady incompressible Navier–Stokes flows. *Journal of Computational Physics*, 2011, 230(17): 6688-6708.
[31] M P Bendsoe, O Sigmund. *Topology optimization: Theory, methods, and applications*. Springer Science & Business Media, 2013.